



Polypropylene with clay–filled for fused filament fabrication: comparative study of the mechanical performance of injected and 3d printed composite

Lina M. Romero¹ · Samir E. Esquivel¹ · Mary C. Montañó² · Carlos Medina-Muñoz³ · Gabriela A. Sánchez-Sanhueza⁴ · Daniel A. Palacio⁵ · Andrés F. Jaramillo^{6,7} · Manuel F. Meléndrez^{1,8}

Received: 14 August 2023 / Accepted: 15 December 2023 / Published online: 15 January 2024
© The Author(s), under exclusive licence to Springer-Verlag London Ltd., part of Springer Nature 2024

Abstract

Fused filament fabrication (FFF) is one of the most used 3D printing techniques; however, the lack of printable materials is its main limitation. Polypropylene (PP) is a promising thermoplastic polymer that offers cost and chemical stability advantages over PLA, but its dimensional instability often leads to poor mechanical performance of printed parts. In this study, a PP filament for FFF was developed, incorporating copper ion-saturated clay (Cu²⁺) and copper oxide nanoparticles (CuO NPs), and the effect of various clay percentages on the tensile properties of the polymer matrix was investigated. The goal was to evaluate the potential use of polypropylene/clay composites as raw materials for FFF. The PP with clay did not form intercalation or exfoliation systems due to the poor matrix-filler interaction, behaving as a microcomposite. Chemical and bactericidal properties were not significantly affected compared to pure PP after the incorporation of clay. However, the thermal stability improved, and the β phase was induced in the crystallization process, enhancing layer adhesion, and reducing deformation during the PP printing process. All injected composites exhibited improved tensile properties, while the opposite effect was observed for printed composites. The best formulation was found for the composite with a 3.0% weight loading of MMT-type II, which showed a 14% increase in tensile modulus for the injected piece and a 17.6% decrease for the printed piece. Despite the reduced mechanical performance in printed pieces compared to injected ones, the material demonstrated processability and printability due to the reduced deformation, which the polymer matrix alone under industrial conditions does not permit.

Keywords Clay · Fused filament fabrication · Mechanical properties · Polypropylene

✉ Manuel F. Meléndrez
mmelendrez@udec.cl

¹ Interdisciplinary Group of Applied Nanotechnology (GINA). Hybrid Materials Laboratory (HML), Department of Materials Engineering (DIMAT), Faculty of Engineering, University of Concepcion, 270 Edmundo Larenas, Box 160-C, 4070409 Concepción, Chile

² Unidad de Docencia y Formación, Universidad Nacional de Colombia – sede Orinoquia, Vía Caño Limón, Kilometro 9, 810001 Arauca, Colombia

³ Department of Mechanical Engineering, University of Concepcion, 219 Edmundo Larenas, Box 160-C, 4070409 Concepción, Chile

⁴ Department of Restorative Dentistry, School of Dentistry, University of Concepcion, 1550 Roosevelt St, 4070409 Concepcion, Chile

⁵ Departamento de Polímeros, Facultad de Ciencias Químicas, Universidad de Concepción, Edmundo Larenas 129, 4070409 Concepción, Chile

⁶ Departamento de Ingeniería Mecánica, Universidad de Córdoba, Cr 6 #76-103, 230002 Montería, Colombia

⁷ Department of Mechanical Engineering, Universidad de La Frontera, 01145 Francisco Salazar, 4780000 Temuco, Chile

⁸ Unidad de Desarrollo Tecnológico, 2634 Av. Cordillera, Parque Industrial Coronel, Box 4051, 4191996 Concepción, Chile

1 Introduction

3D printing has emerged as a widely adopted manufacturing method across various industrial sectors due to its ability to produce materials with complex three-dimensional shapes quickly and cost-effectively [1]. This approach involves the progressive construction of objects by stacking and fusing layers of material using computer programs [2]. Compared to subtractive techniques, 3D printing offers customization, cost savings, time efficiency, and waste minimization, thus becoming a valuable technology, especially in the biomedical field [3, 4].

Despite the significant advantages offered by 3D printing, some techniques like fused filament fabrication (FFF), widely used in rapid prototyping due to its low cost, speed, and simplicity compared to other 3D printing methods [5], present limitations that have hindered its widespread implementation in the industry. The main limitation of FFF lies in its thermo-driven nature, which restricts its application to a limited number of polymers with specific thermal and mechanical properties to ensure dimensional stability and prevent polymer degradation during the printing process [6]. Therefore, the current focus is on developing composite materials with necessary mechanical and thermal properties to meet different printing and processing requirements, without compromising the simplicity and low cost that characterize FFF [7].

Among thermoplastic polymers, polypropylene (PP) has gained interest due to its low cost, recyclability, ease of processing, and chemical stability, surpassing more conventional materials like polylactic acid (PLA) and acrylonitrile butadiene styrene (ABS) in these areas [8, 9]. However, its use in FFF has been limited by excessive shrinkage during the printing process, affecting dimensional stability and surface adhesion, thereby impacting the mechanical properties of printed parts or preventing complete piece printing. To overcome these challenges, numerous studies have been conducted to improve PP's dimensional stability during 3D printing and the mechanical properties of printed parts.

For instance, Aumnate et al. [9] reinforced PP with polylactic acid-graphene microcapsules, demonstrating that 3D printed structures with 30% filling (weight/weight) exhibited better mechanical performance compared to pure PP. On the other hand, Stoof and Pickering [10] achieved an 84% reduction in pure polypropylene shrinkage by adding 30% harakeke filling. Additionally, studies on FFF 3D printing of PP have reported that shrinkage can be controlled by adding fillers and manipulating the temperature in the build chamber [11, 12]. These findings highlight the feasibility of reinforcing PP with fillers for FFF 3D printing, improving both the mechanical properties

and dimensional stability of 3D printed PP parts. In this regard, montmorillonite clay (MMT), a low-cost mineral filler with a structure allowing it to act as an ion carrier [13], has generated particular interest in reinforcing PP due to significantly enhancing mechanical properties compared to the pure polymer. Furthermore, the nucleating effect of MMT layers in the polymeric matrix enhances PP crystallization, thereby reducing excessive shrinkage during printing.

For example, Chikkangoudar et al. [4] conducted 3D printing of polypropylene and nanometric clay using laser scanning, demonstrating that inclusion of nano-clay improved the dimensional flexibility of polypropylene, significantly reducing deformation in 3D printed models. However, they observed increased fragility of filaments and 3D models with higher percentages of nano-clay. In another research, Aumnate and team [14] investigated the effects of organoclay and the compatibilizer dioctadecyl dimethylammonium chloride (D18) on thermal, rheological, and morphological properties to assess the viability of polypropylene/organo-clay nanocomposites as raw materials for FFF 3D printing. Their findings indicated that MMT inclusion reduced volatility and dimensional shrinkage of PP, enabling its 3D printing.

Despite significant advances that have made PP a promising material for FFF and recognizing the reinforcement of its polymeric matrix with fillers as an effective solution for these challenges, simultaneous improvement of its mechanical properties and dimensional stability remains crucial. It has been observed that a significant reduction in shrinkage can lead to increased material fragility, and vice versa [10]. This duality has hindered its effective implementation in FFF 3D printing. Therefore, it becomes imperative to conduct more detailed research to find an optimal balance between these factors. This advancement would be fundamental in creating a material truly suitable for industrial applications.

Furthermore, in the biomedical field, bacterial adhesion on rough surfaces of 3D prints poses a health risk [15]. Hence, it is vital that structures are not only mechanically functional but also possess antimicrobial properties. The incorporation of metallic ions and nanoparticles has been studied to prevent bacterial adhesion and proliferation on printed piece surfaces. Copper is one of the most commonly used antimicrobial metallic ions in the form of micro/nanoparticles due to its angiogenic activity [16]. Moreover, they have been combined with metal oxide nanoparticles such as copper oxide (CuO) to enhance and prolong their effect, as nanoparticles have a higher surface-to-volume ratio, providing more contact surface with the environment and acting as ion reservoirs [17].

This study focuses on the development of polypropylene filaments with copper ion-loaded clay and copper oxide nanoparticles for 3D printing using the FFF technique. The

mechanical performance of the printed composite material was evaluated through tensile tests, comparing it with the injected material, aiming to explore the potential of PP/MMT (Cu/CuO) composites as materials for FFF 3D printing. This study aims to contribute to understanding the enhancement of mechanical properties and dimensional stability of 3D printed PP, as well as its potential application in various industrial areas, including the biomedical sector [1–17].

2 Materials and methods

2.1 Reagents

The natural montmorillonite clay, MMT, was obtained from OREGON CHEM GROUP (Santiago, Chile) and used as an additive. Its main physical and chemical properties are shown in Table S1. Sulfuric acid (H_2SO_4 , 98%), copper sulfate pentahydrate ($\text{CuSO}_4 \cdot 5\text{H}_2\text{O}$, 99.8%), and glycerin ($\text{C}_3\text{H}_8\text{O}_3$, 85%, plasticizer) were obtained from Merck (Santiago, Chile). Copper oxide (CuO) nanoparticles were supplied by US Research Nanomaterials Inc. (Houston, TX, USA). The isotactic homopolymer PP (MFI = $27 \text{ g } 10^{-1} \text{ min}^{-1}$) in granular form was supplied by PETROQUIM S.A (Santiago, Chile).

2.2 Saturation of MMT with copper ions

The MMT saturation with copper ions (Cu^{2+}) was achieved through a chemical activation process of the MMT to obtain the best cation exchange capacity (CEC) for copper ions (see Supplementary Information S1). Subsequently, the effect of MMT and A-MMT dosage, as well as the initial metal concentration, was evaluated. Batch experiments were conducted using $\text{CuSO}_4 \cdot 5\text{H}_2\text{O}$ (99.8%) solutions under constant agitation (200 rpm) for 24 h. Samples with MMT contents of 0.1, 0.25, 0.50, 0.75, 1.0, and 2.0 g were added to a Cu^{2+} solution of 13.5 g L^{-1} . To assess the effect of the initial concentration of Cu^{2+} ions, concentrations varied between 5, 10, 15, 20, 30, 40, and 50 g L^{-1} with a constant amount of clay. Each batch was centrifuged, and the remaining Cu^{2+} concentration was analyzed in triplicate using an atomic absorption spectrophotometer, Model 800 (Perkin-Elmer Analyst, MA, USA). Finally, the samples were dried at $60 \text{ }^\circ\text{C}$ for 24 h, followed by milling and sieving ($< 125 \mu\text{m}$). The resulting product was named MMT-type II and was characterized by Fourier-transform infrared spectroscopy (FT-IR) using a Nicolet model (Thermo Fisher Scientific, MA, USA).

2.3 Obtaining MMT with supported CuO NPs

Commercial CuO NPs ($798 \text{ g Cu}^{2+} \text{ kg}^{-1}$) were supported on the surface of MMT-type II ($3.5 \text{ g Cu}^{2+} \text{ kg}^{-1}$) through solid-state mechanical agitation, and the mixture was homogenized using a mortar. It was added at a weight ratio of 1:7 (CuO NPs: MMT-type II) to achieve a maximum copper concentration of 100 g kg^{-1} . The resulting mixture was named MMT-type I. To determine the shape and size of the supported nanoparticles, a transmission electron microscope (TEM), Philips Tecnai 12 (Eindhoven, NL), was used, and FT-IR characterization was performed.

2.4 Obtaining the Masterbatch of polymeric composites and filament manufacturing

To produce the masterbatch (MB), PP was physically mixed with 5 wt% of MMT-type I and MMT-type II, separately, along with 1.5 wt% of glycerin (see Table S2). The MB was mixed in a molten state using a twin-screw extruder (Baopin, Dongguan, China). The extruder temperatures were set from 180 to $210 \text{ }^\circ\text{C}$ with an increase of $10 \text{ }^\circ\text{C}$ per zone, keeping $210 \text{ }^\circ\text{C}$ for the fifth zone and reducing by $20 \text{ }^\circ\text{C}$ at the nozzle zone, with a rotation speed of 50 rpm. Finally, the MB was diluted to 3.0 and 1.0 wt% of MMT, and the composites were obtained in granular form. The filaments were manufactured using a continuous extrusion/winding system integrated with a diameter sensor. The polymeric composites in granular form, filaments, and injected and printed parts were labeled as follows: PP/MMT-type I (1%); PP/MMT-type I (3%); PP/MMT-type I (5%); PP/MMT-type II (1%); PP/MMT-type II (3%) and PP/MMT-type II (5%). These labels indicate the different combinations of polypropylene (PP) with either MMT-type I or MMT-type II at 1, 3, and 5 wt% of the respective type of clay in the polymeric matrix.

2.5 Manufacture of composite materials

2.5.1 Injection molding

The manual injector (Model 150A PLASTIC INJECTION MACHINE, LNS TECHNOLOGIES, USA) was used to manufacture all the composites by injection, following these steps and conditions: mold preheating ($80 \text{ }^\circ\text{C}$, 3 min) and composite heating ($200 \text{ }^\circ\text{C}$, 1.5 min), injection, and cooling ($20 \text{ }^\circ\text{C}$, 0.5 min). The mold used was V-type traction test specimens (ASTM D638) [18].

2.5.2 3D printing process

The FFF 3D printer Artillery (Shenzhen Yuntuchuangzhi Technology Co., China) was used to print all the composites, with the parameters shown in Table 1. The printed parts

Table 1 3D printing parameters for FFF of the different PP/MMT composite

Parameters*	Values
Nozzle temperature, °C	220
Build plate temperature, °C	110
Printing speed, mm s ⁻¹	40
Fill percentage, %	100
Flow rate, %	120
Retraction	Not enabled
Supports	Not required
Direction	45° and 135°, alternating
Fill type	Linear
Adhesion to the build plate	Skirt, 15 mm
Print quality—layer height	Standard quality—2 mm

* The printing parameters were selected based on previous research [10, 12, 14], which were then adapted for our material through cantilever and stepping tests. However, determining the specific optimal printing parameters for this material is beyond the scope of this research.

were V-type traction test specimens (ASTM D 638) and specimens for contraction testing (Figure S1). In Figure S2 and Table S3, the experimental matrix detailing the manufacturing process of the PP/MMT composites is presented.

2.6 Characterization of the composites

The dispersion of the clay in the polymer matrix was figured out using X-ray diffraction (XRD) and scanning electron microscopy (SEM) micrographs. Regarding the thermal properties, a thermogravimetric analysis (TGA) was performed using a NETZSCH TG 209F3 Thermal Analyzer to study the thermal stability of the composites. The TGA was conducted with a heating rate of 10 °C min⁻¹ from 25 to 600 °C, under an inert atmosphere (N₂). Additionally, a differential scanning calorimetry analysis (DSC) was conducted using a NETZSCH DSC 204F1 Phoenix instrument to determine the melting temperature and crystallinity percentage. The DSC analysis was performed under a nitrogen atmosphere in a range of 25 to 200 °C. The samples were heated to 220 °C for 5 min to erase the thermal history, cooled to 40 °C, and then heated again to 220 °C. A scanning rate of 10 °C min⁻¹ was used for all steps. To determine the variation in the resistance of the composites compared to pure PP when exposed to chemical agents, a chemical resistance test based on ASTM D543 standard was conducted, specifically in the immersion test: Procedure I—Weight and Dimensional Changes. The reagents used were hydrochloric acid (HCl, 10 wt%), sodium hydroxide (NaOH, 10 wt%), and ethanol (Et-OH, 95 wt%) [19]. Similarly, to determine the variation in water absorption of the composites compared to pure PP when immersed in water, a water absorption test based on ISO 62 standard was conducted, specifically

Table 2 Comparison of the adsorption efficiency of copper ion on activated and natural clay

Clay – MMT	Adsorption percentage (%)	Adsorption capacity (mg g ⁻¹)
	Cu ²⁺	Cu ²⁺
Natural MMT	36.70	98.03
Activated MMT	11.10	29.59

Method 1: Determination of the amount of water absorbed after immersion in water at 23 °C [20].

2.7 Tensile test

The tensile test was conducted on a ProLine universal testing machine (ZwickRoell, Germany) at a constant deformation rate of 50 mm min⁻¹. The tensile modulus, tensile strength, and elongation at break were evaluated using V-type geometry specimens according to ASTM D 638 standard, and the arithmetic mean of five replicates was reported.

2.8 Antibacterial assay: kinetics of bacterial killing

This procedure is described in Supplementary Information S2.

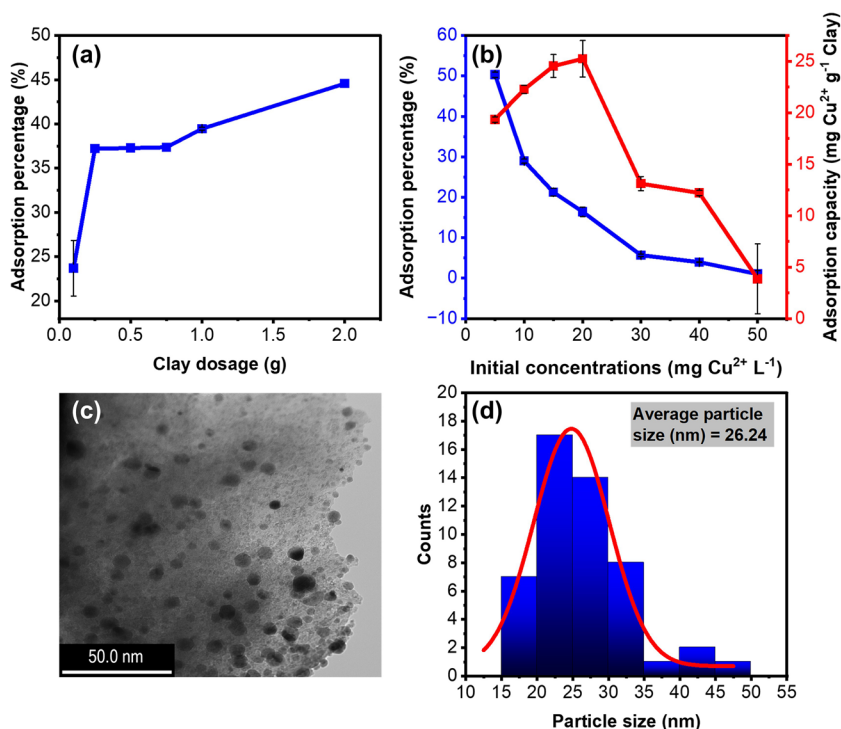
3 Results and discussion

To remove impurities, increase porosity, and enhance the copper ion adsorption process, a thermo-acidic activation was performed on the clay (the characterization of the clay before and after the thermo-acidic activation is presented and discussed in the supplementary information S3 and Figure S3). The efficiency of A-MMT in ion adsorption was determined by contacting it with a copper ion solution. The natural clay showed better adsorption performance than the activated clay, due to a sharp decrease in pH in A-MMT that is difficult to control after the activation process (see Table 2). This could be due to the competition between the excess of hydrogen ions and the metallic ions for the same active sites, which can easily become protonated and suppress the adsorption of metallic ions. This pH effect on copper ion adsorption was reported by Pawar et al. [21]. Based on these results, it was concluded to use the natural clay (MMT) as the filling agent.

3.1 Study of the maximum adsorption capacity of copper ions and support of CuO NPs in MMT

The percentage of metal ion adsorption with respect to the MMT dosage is shown in Fig. 1a. The adsorption efficiency increases as the amount of clay increases. This

Fig. 1 **a** Effect of adsorbent dosage for Cu^{2+} adsorption, **b** effect of initial metal concentration, **c** TEM image of CuO NPs supported on MMT-type II, and **d** histogram of particle size distribution of CuO NPs in MMT-type II



phenomenon can be explained by the increase in the MMT's surface area, which may be related to a higher availability of active sites on the MMT. The initial concentration of metal ions in the solution played a significant role as a driving force to overcome mass transfer resistance between the aqueous and solid phases, hence it was varied between 5.0 and 50.0 g L $^{-1}$ of copper ions using 2.0 g of MMT. The results are represented as the percentage of adsorption against the initial concentration of copper ions and the adsorption capacity (see Fig. 1b). As the concentration of ions in solution increases, the percentage of adsorption decreases. This is because the availability of active sites on the surface of MMT decreases as the concentration of ions in solution increases. However, the adsorption capacity gradually increased until reaching the maximum ion exchange capacity of MMT. The highest ion exchange capacity occurs at a concentration of 20.5 g Cu^{2+} L $^{-1}$, with an exchange of 25.5 mg of copper per 1 g of MMT. These results indicate that at higher concentrations of metal ions, the high ion collisions, and diffusion speed lead to a lower percentage of adsorption [21]. Similar findings were reported by Xiaoying et al. [22] and Ding et al. [23], Similarly, they reported that the Cu^{2+} adsorption capacity in MMT is 22 and 26 mg g $^{-1}$, respectively. Using this information, we obtained the first additive, copper-saturated montmorillonite clay (MMT-type II), with a copper concentration of 3.5 g kg $^{-1}$, from a Cu^{2+} solution of 20.5 g L $^{-1}$.

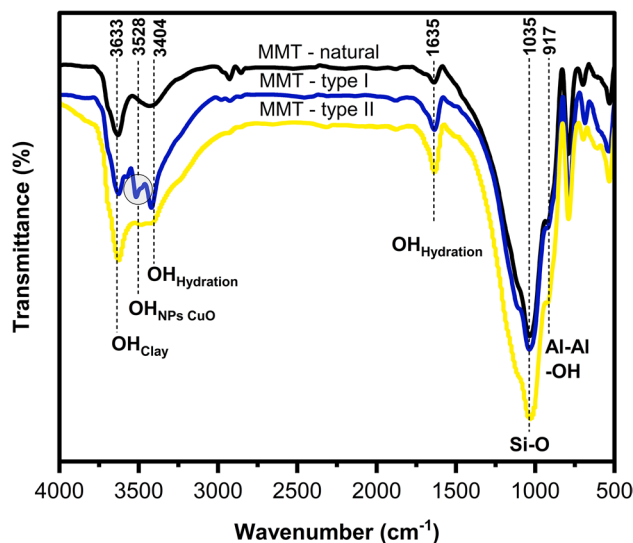


Fig. 2 FT-IR spectra of the MMT before and after adsorption of Cu^{2+} ions and Cu^{2+} ions + CuO NPs

In Fig. 1c, the TEM image shows that CuO-NPs were supported on the surface of MMT-type II. Meanwhile, the solid-state physical mixing improved the particle size, with an average particle size of 26.0 nm (see Fig. 1d). In this way, the second additive, copper-saturated clay with supported CuO NPs (MMT-type I), was prepared with a copper concentration of 100 g kg $^{-1}$.

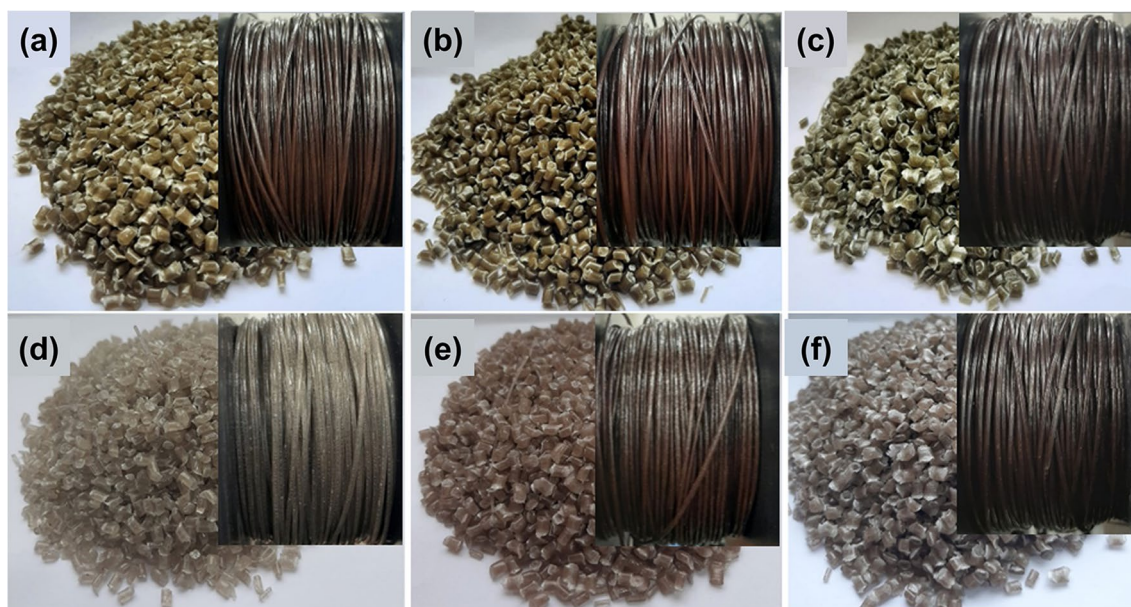


Fig. 3 Filaments of the composites: **a** PP/MMT-type I (1%); **b** PP/MMT-type I (3%); **c** PP/MMT-type I (5%); **d** PP/MMT-type II (1%); **e** PP/MMT-type II (3%); and **f** PP/MMT-type II (5%)

3.2 Characterization of additives

The additives, MMT-type II and MMT-type I, were analyzed by FT-IR (see Fig. 2). In general, an increase in intensity around 1632 cm^{-1} associated with the vibrations of -OH groups were observed compared to MMT, indicating the adsorption of copper and NPs through the hydration process [24]. Similarly, at 1032 cm^{-1} , the band associated with stretching (Si-O) showed modifications both in intensity and amplitude. These variations are related to structural changes in the MMT due to the ion exchange of ions and NPs with different chemical properties. In the spectrum of MMT-type I, it shows higher intensity compared to that of MMT-type II, attributed to a greater disposition of the NPs on the surface of MMT due to their nanoscale size, allowing them to intensify Van der Waals interactions between the oxygen groups of MMT and the NPs [25, 26].

3.3 Characterization of the composites PP/MMT-type II and PP/MMT-type I

In general, all the composites, PP/MMT-type I (1%); PP/MMT-type I (3%); PP/MMT-type I (5%); PP/MMT-type II (1%); PP/MMT-type II (3%) and PP/MMT-type II (5%), had an average filament diameter of 1.5 mm. Although it is below the commercially needed size, it showed consistency in diameter throughout the process (see Fig. 3).

To determine the system formed between the polymer matrix and the clay, diffractograms are presented in Fig. 4. MMT-type I and MMT-type II show a main peak

at $2\theta = 7.11$ and 6.96° , corresponding to the interlayer spacing $d_{001} = 12.41$ and 12.67 \AA , respectively. Meanwhile, PP shows its main peak at $2\theta = 14^\circ$, corresponding to $d_{110} = 6.3\text{ \AA}$ (see Fig. 4a). It is clear that the proposed additives did not produce polymer chain intercalation or clay layer exfoliation (see Fig. 4b–c). The immiscibility of polypropylene with a hydrophilic clay is expected; furthermore, it is seen that in both classes of composites, as the percentage of clay decreases, the systems behave better in terms of interlayer distances, since at lower percentages, the immiscibility between PP and clay is reduced [27]. Composites are systems of separate phases that only lead to microcomposites [27, 28].

In Fig. 5, micrographs for morphological study are shown. It can be seen that as the percentage of clay increases, there is a tendency for clay particles to form agglomerates. This is a result of the unmodified clay sheets having a high surface energy and being bound together by electrostatic interactions, forming aggregates due to the higher affinity between clay particles compared to the polymer matrix [28]. For the 1 wt% clay content (Figs. 5c–f), no clay aggregates were seen, suggesting good dispersion of the clay in the PP matrix, which is consistent with the XRD results. For higher clay contents (Figs. 5a–b, d–e), a rough surface with some micrometer-sized aggregates is seen, showing a weak interfacial bond between MMT and the PP matrix, significantly reducing the ability to accept large plastic deformations [29].

Furthermore, a lack of high shear during the melt mixing process was considered. On the other hand, it was observed that the clay saturated with copper showed a more

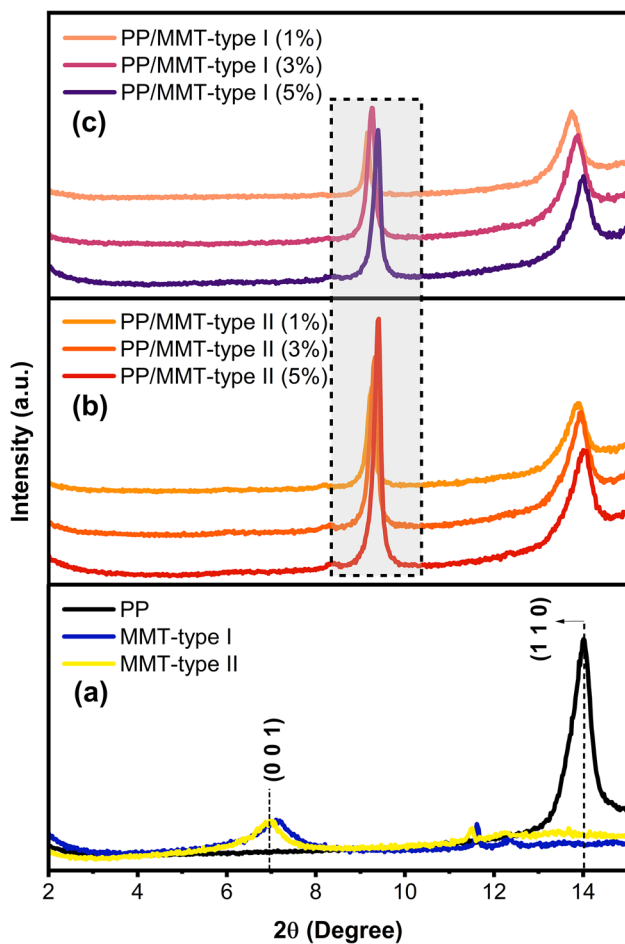


Fig. 4 X-ray diffractograms of **a** PP and clay types, **b** PP/MMT-type II composite, and **c** PP/MMT-type I composite

homogeneous dispersion in the polymer matrix than the one saturated with both copper and copper oxide nanoparticles. This could be because the addition of copper oxide nanoparticles with high surface energy promotes the formation of more aggregates. The presence of clay aggregates could be responsible for the lower increase in the tensile modulus as the clay content increases, and this will be further detailed later.

3.4 Thermal properties

Understanding the thermal stability of materials to be processed by FFF is crucial due to the successive heating cycles the material undergoes during the printing process. Therefore, the temperature of thermal degradation can limit the processing conditions of the material. The effect of the clay content (MMT) on the thermal degradation behavior of the composites is shown in Fig. 6, and the derived data is presented in Table S4. The thermal stability of the materials can be enhanced by the addition of rigid fillers, as evidenced

in the composites PP/MMT-type I (1%) and PP/MMT-type II (5%), which increased the maximum degradation temperature by 6 °C and 5 °C, respectively, compared to pure PP. This could be attributed to the presence of fillers with a high aspect ratio (CuO-NPs) homogeneously dispersed, which, along with the MMT particles, prevent the evolution of volatile substances, acting as a barrier that inhibits the heat propagation from the environment within the polymeric matrix [30, 31]. However, the composites with 3 and 5 wt% MMT-type I showed lower thermal stability compared to PP. The poor interaction between MMT and PP led to clay agglomerates with micrometric particles and a low aspect ratio, resulting in short pathways that increased the diffusion of volatile substances, thereby limiting the barrier property [32]. The previous results confirmed that the stability of PP could be improved by incorporating MMT when there is a homogeneous dispersion of particles with a high aspect ratio within the polymeric matrix. Therefore, material degradation during processing can be avoided.

In FFF, the thermoplastic polymer is extruded through a nozzle with a temperature higher than the material's melting temperature. This is done to form smooth strands and build the designed piece. Additionally, it helps promote adhesion between the deposited layers by delaying the crystallization process. However, exposing the material to a temperature significantly higher than its melting point can lead to material degradation. On the other hand, a rapid crystallization process may result in voids between the deposited layers, affecting the mechanical behavior and causing deformation of the piece due to accumulated residual stresses [14, 32, 33]. To study the effect of MMT on the crystallization process and the melting temperature, the DSC curves for PP/MMT-type II and PP/MMT-type I are shown in Fig. 7, and the derived properties from these curves are given in Table S5. The PP showed a melting temperature of 169.4 °C, characteristic of α -phase crystals, which varied slightly in all composites, but not significantly [34] (see Fig. 7a). Due to the lack of polymer diffusion between the clay layers, the melting temperature strongly depended on the polymer matrix. However, this variation indicates that the incorporation of MMT could modify the polymer's crystalline structure [35]. All composites showed the presence of a new peak at 130 °C, corresponding to the melting of β crystals [36]. As evident in the diffractogram (see Fig. 7b), a peak appears at 18.9° corresponding to the (301) reflection of the β phase [37].

On the other hand, as the clay content in the polymer matrix increased, there was a decrease in the crystallization percentage (see Table S4), because the MMT hinders the folding of macromolecular chains and limits the space for nucleation/growth of crystals [38]. Therefore, the barrier effect was dominant in the crystallization process. Meanwhile, for the enthalpy of fusion, the values decrease with

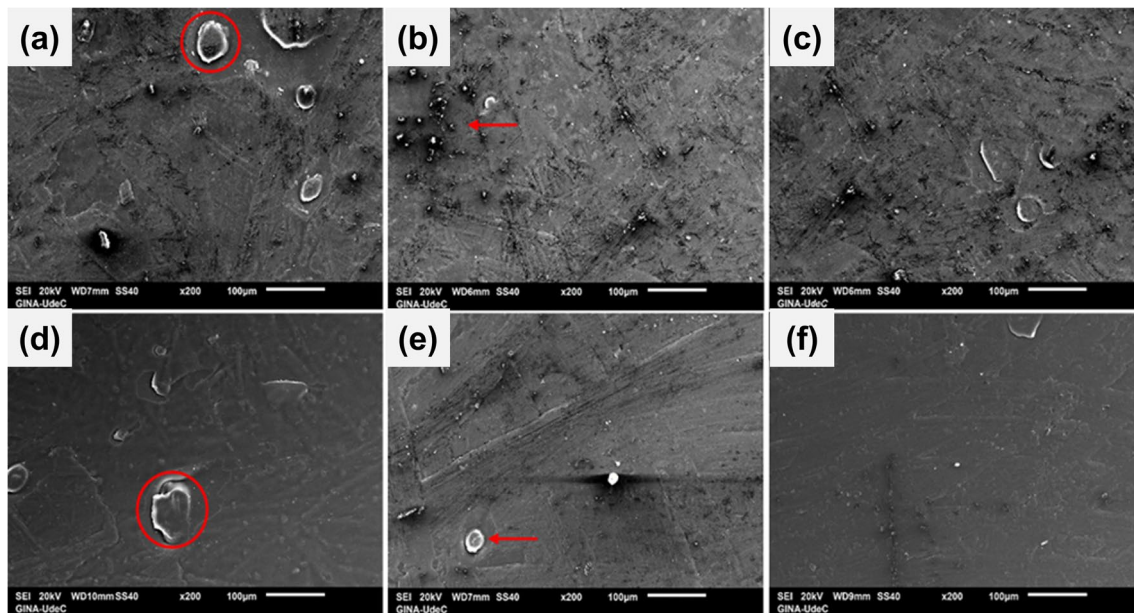


Fig. 5 SEM micrographs of the composites: **a** PP/MMT-type I (5%); **b** PP/MMT-type I (3%); **c** PP/MMT-type I (1%); **d** PP/MMT-type II (5%); **e** PP/MMT-type II (3%); **f** PP/MMT-type II (1%)

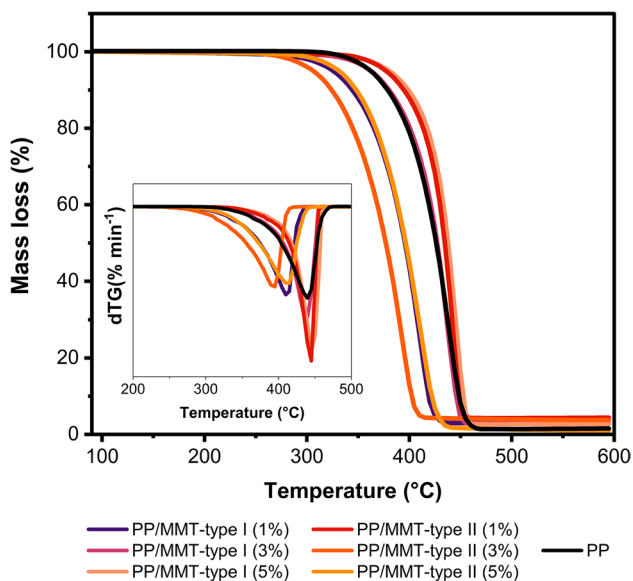


Fig. 6 Thermal stability was evaluated by TGA-dTG

the addition of clay compared to PP; this phenomenon can be attributed to a decrease in the content of thermodynamically stable α phase in favor of a mesomorphic structure [31]. These results suggest that the appearance of the β phase induced by MMT can improve the sensitivity of PP to the thermal memory effect in 3D printing, and the melting point of the composites close to polymers like PLA indicates that these composites can be printed using conventional printers.

3.5 Mechanical properties

To measure the mechanical properties, the elastic modulus (a), the yield strength (b), and the fracture strain (c) are studied, see Fig. 8. In Figure S4, the injected and 3D-printed specimens are shown before and after the test, along with the stress–strain curve (see Figure S5). In Fig. 8 a, it can be seen that the addition of clay increases the elastic modulus in all the injected composites, resulting in an enhancement of material stiffness. The significant increase was 14% for composite PP/MMT-type II (3%) and 9.7% for composite PP/MMT-type I (5%) compared to PP. For the same printed composites, there was a decrease in the elastic modulus compared to the injected PP of 17%. This is because three-dimensional printing does not apply pressure during the formation of the piece, which can create voids in the layer bonding, distorting the test. This behavior was like what was studied by Carneiro et al. [39] in PP composites with fiberglass, where samples produced through 3D printing showed a decrease of around 30% compared to those produced by compression molding. This suggests that the degradation is not due to poor filament adhesion but rather the presence of voids (poor compaction) in the samples. Furthermore, it was seen that the composites, regardless of the type of MMT used, become more brittle with a content higher than 3 wt% of MMT. This could be attributed to the non-homogeneous dispersion of MMT (see Fig. 5). This effect tends to slow down the increase in material stiffness as defects at the interface intensify due to internal stresses, which can lead to the formation of small cracks during the stress–strain

Fig. 7 **a** DSC heating curves and **b** XRD of PP/MMT composites

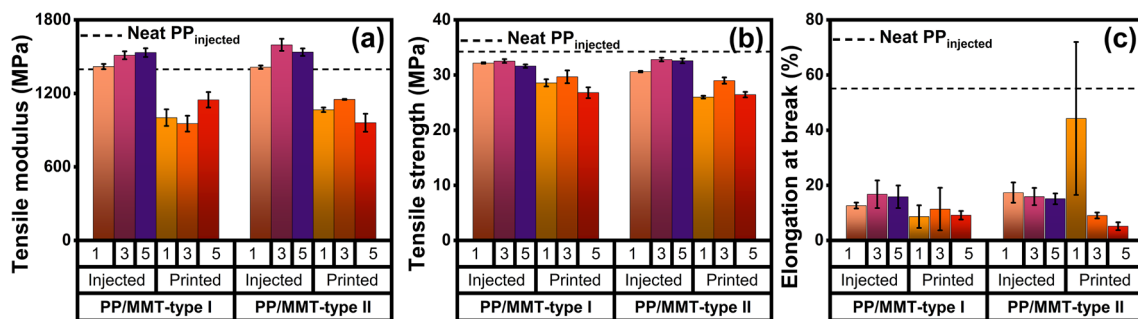
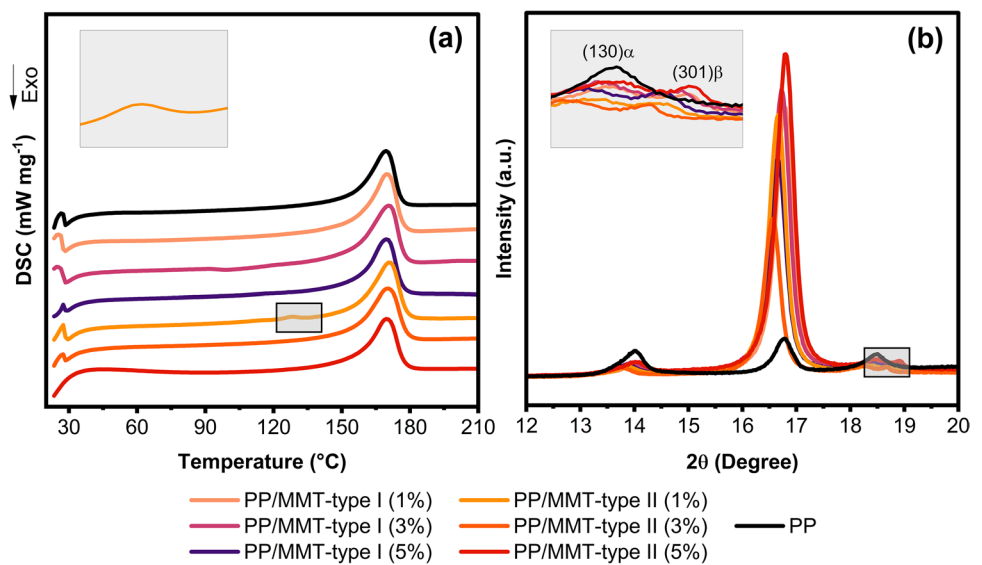


Fig. 8 Mechanical properties according to ASTM D638 of injected and printed composites: **a** Tensile modulus, **b** tensile strength, and **c** elongation at break

test. Part of the mechanical energy is then used in the formation of these cracks [30].

In Fig. 8b, it is seen that the maximum strength decreases in all the injected and printed composites due to poor matrix-filler interaction, resulting in the absorption of all applied stress by the polymer matrix. Additionally, the filler hinders the interaction between chains, leading to a decrease in intermolecular interactions and, so, the material's strength [40]. This suggests that the composites are brittle materials.

Regarding fracture strain, Fig. 8c shows a drastic decrease in all the composites, with a general reduction of 85.0%, which decreases as the clay percentage increases. This decrease is attributed to the strong restriction imposed by the clay on the movement of polymer chains when subjected to stresses, preventing them from elongating and reducing elasticity [40, 41]. This effect intensifies when there is poor filler–polymer interaction. Furthermore, the reduction in elastic material (polymer) due to the presence of inelastic material (filler) is consistent.

Hence, the composites containing 1 and 3 wt% of MMT exhibit excellent tensile properties, which aligns consistently with the findings reported in [14, 31]. Moreover, the type of additive used does not exert a considerable influence on the tensile tests. It is noteworthy that the 3D printed FFF composites developed in this study highlighted superior mechanical performance compared to those reported by Aumnate et al. [14]. Unlike their approach, which incorporated organically modified clay and compatibilizer in the mixture, our method stands out as a distinct and promising alternative. The contraction of printed parts is an important aspect of mechanical performance in FFF printing, as it can disrupt the printing process. Because the printed parts exhibited contraction, the behavior of PP was analyzed based on the percentage of MMT, by measuring the separated part of the print from the printing bed. For this, measurements were taken using a Vernier caliper micrometer, and the reported values are an average of five measurements. In Fig. 9, the parts of the different composites can be observed showing contraction, with a decrease in

Fig. 9 **a** Printed parts of the PP/MMT-type I and PP/MMT-type II composites. The pieces show significant deformation that progressively reduces as the MMT content in the mix increases; **b** Deformation in printed parts of PP/MMT-type I and PP/MMT-type II composites as a function of the increase in the percentage of MMT

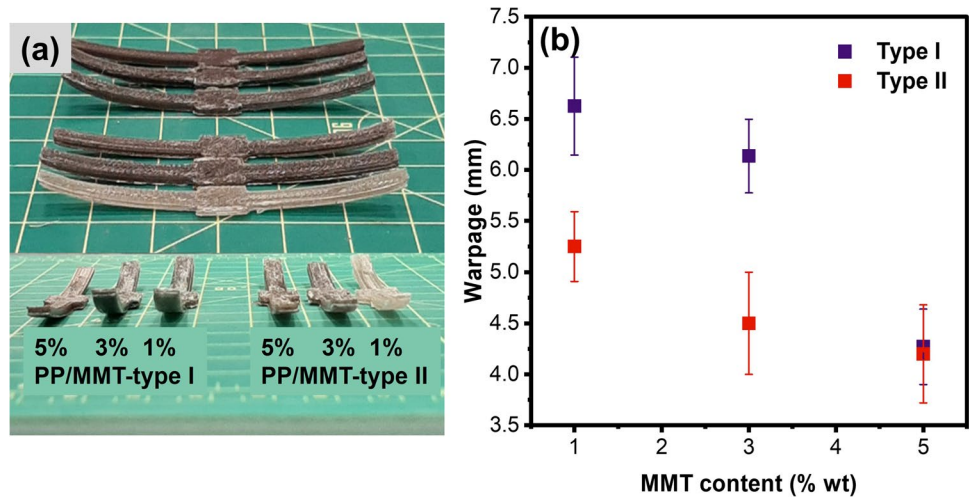
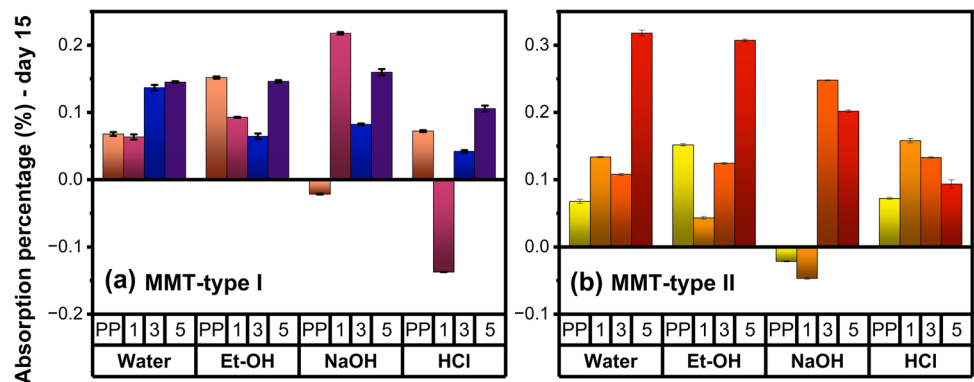


Fig. 10 Water absorption (ISO 62) and chemical resistance (ASTM D543) of PP and PP/MMT composites: **a** MMT-type I and MMT-type II



contraction as the load increases (see Fig. 9a–b). This indicates that upon solidification, the polymer chains experience restrictions that prevent abrupt changes in free volume, which aligns with the parameter of fracture elongation (see Fig. 8c) in the contraction test [41, 42].

Notably, the MMT-type II composites exhibit less contraction compared to MMT-type I, thanks to better dispersion (see Fig. 5). Therefore, in terms of tensile modulus and contraction parameter, PP/MMT-type II composites outperform PP/MMT-type I. Although complete elimination of contraction was not achieved, it was significantly reduced compared to pure PP, which is not printable using this technique under industrial conditions.

3.6 Chemical properties

Water absorption can influence the mechanical properties of materials, while chemical resistance is essential in determining their application. Figure 10 shows the behavior of PP and all the composites when submerged in water and different reagents. All the composites exhibited a higher percentage of water and reagent absorption compared to PP, but

the increase was not significant. This slight increase can be attributed to the affinity between the dispersed phase (clay) and water, as well as the polar reagents used, with the uncovered O or OH adsorption sites in the composites. Therefore, a higher clay content was reflected in a higher absorption percentage [43, 44].

Another factor favoring water and reagent absorption is the weak or non-existent interfacial bonding between the clay particles and the PP matrix. The interfacial zone serves as a privileged pathway for the migration of small molecules. Thus, diffusivity is an increasing function with respect to the clay loading content [28, 44]. Although the difference between the MMT-type II and MMT-type I additives is not significant.

3.7 Evaluation of antibacterial properties

The bactericidal, bacteriostatic, or inactivity of PP/MMT modified composites over time against bacterial strains *Staphylococcus aureus* UCO 99 (a) and *Acinetobacter baumannii* UCO 538 (b) is shown in Figure S6. As observed in Figure S6, none of the composites exhibited bactericidal or bacteriostatic activity. This result could be attributed to

the insufficient copper concentration in the clay, which did not allow the composites to display an antimicrobial effect. Additionally, the low percentages of clay in the composites contributed to this outcome. MMT-type II was supported with 3.5 g L^{-1} of copper, and when incorporated into the polymer matrix at the highest percentage (5%), only 0.175 g L^{-1} of copper remained. Literature has indicated that *Staphylococcus aureus* is sensitive to 5 g L^{-1} of Cu^{2+} [45]. Therefore, MMT-type I was increased to a concentration of 100 g L^{-1} , but it still did not show either of the expected effects. This is attributed to material loss during processing, primarily in extrusion, or inadequate release of CuO NPs.

4 Conclusions

The results prove that the 3D printing process of polypropylene (PP) can be improved by incorporating low percentages of a mineral additive, derived from economical and sustainable processes. Among the proposed additives, the inclusion of MMT-type II reduced the contraction of the printed composites, which is a crucial factor during the printing process, compared to the MMT-type I additive. These additives functioned as beta-type nucleating agents, inducing the growth of such crystals, which affected the nucleation process and allowed for the printing of more dimensionally stable parts compared to PP.

Although the tensile properties of the printed parts decreased compared to the injected pieces and complete elimination of contraction was not achieved, these results suggest that PP can be 3D printed using FFF without significant contraction effects. Key considerations include fusion mixing, where shear plays a key role in clay dispersion, affecting the mechanical performance of the final products, without the need for added additives or processes such as raw material functionalization.

Supplementary Information The online version contains supplementary material available at <https://doi.org/10.1007/s00170-023-12889-7>.

Author contribution Lina M. Romero: Investigation, Methodology, Validation, Writing—Original Draft. Samir E. Esquivel: Investigation, Methodology, Validation. Mary C. Montaña: Writing—Review and Editing. Carlos Medina–Muñoz: Resources, Funding acquisition, Project administration, Conceptualization. Gabriela A. Sánchez–Sanhueza: Investigation, Methodology, Validation. Daniel A. Palacio: Writing—Review and Editing. Andres F. Jaramillo: Writing—Review and Editing. Manuel F. Meléndrez: Conceptualization, Supervision, Writing—Review and Editing.

Funding This work was funded by the FONDEF project ID20I10040 of the National Agency for Research and Development (ANID), Ministry of Science, Government of Chile.

Declarations

Ethics approval Not applicable.

Consent to participate Not applicable.

Consent for publication All the authors declare their consent for the publication of the manuscript after acceptance.

Competing interests The authors declare no competing interests.

References

- Kabir SMF, Mathur K, Seyam AFM (2020) A critical review on 3D printed continuous fiber-reinforced composites: history, mechanism, materials and properties. *Compos Struct* 232 <https://doi.org/10.1016/j.compstruct.2019.111476>
- Germaini MM, Belhabib S, Guessasma S, Deterre R, Corre P, Weiss P (2022) Additive manufacturing of biomaterials for bone tissue engineering – a critical review of the state of the art and new concepts. *Prog Mater Sci* 130 <https://doi.org/10.1016/j.pmatsci.2022.100963>
- Liu S, Lu B, Li H, Pan Z, Jiang J, Qian S (2022) A comparative study on environmental performance of 3D printing and conventional casting of concrete products with industrial wastes. *Chemosphere* 298: <https://doi.org/10.1016/j.chemosphere.2022.134310>
- Chikkangoudar RN, Sachidananda TG, Pattar N (2020) Influence of 3D printing parameters on the dimensional stability of polypropylene/clay printed parts using laser scanning technique. In: *Materials Today: Proceedings* <https://doi.org/10.1016/j.matpr.2020.10.456>
- Jadhav A, Jadhav VS (2022) A review on 3D printing: an additive manufacturing technology. *Mater Today Proc* 62: <https://doi.org/10.1016/j.matpr.2022.02.558>
- Monzón MD, Gibson I, Benítez AN, Lorenzo L, Hernández PM, Marrero MD (2013) Process and material behavior modeling for a new design of micro-additive fused deposition. *Int J Adv Manuf Technol* 67: <https://doi.org/10.1007/s00170-012-4686-y>
- Vaes D, Van Puyvelde P (2021) Semi-crystalline feedstock for filament-based 3D printing of polymers. *Prog Polym Sci* 118 <https://doi.org/10.1016/j.progpolymsci.2021.101411>
- Vidakis N, Petousis M, Velidakis E, Mountakis N, Fischer-Griffiths PE, Grammatikos SA, Tzounis L (2022) Fused Filament Fabrication 3D printed polypropylene/ alumina nanocomposites: effect of filler loading on the mechanical reinforcement. *Polym Test* 109:107545. <https://doi.org/10.1016/j.polymertesting.2022.107545>
- Aumnate C, Potiyaraj P, Saengow C, Giacomini AJ (2021) Reinforcing polypropylene with graphene-poly(lactic acid) microcapsules for fused-filament fabrication. *Mater Des* 198:109329. <https://doi.org/10.1016/j.matdes.2020.109329>
- Stoof D, Pickering K (2018) Sustainable composite fused deposition modelling filament using recycled pre-consumer polypropylene. *Compos B Eng* 135:110–118. <https://doi.org/10.1016/j.compositesb.2017.10.005>
- Spoerk M, Sapkota J, Weingrill G, Fischinger T, Arbeiter F, Holzer C (2017) Shrinkage and warpage optimization of expanded-perlite-filled polypropylene composites in extrusion-based additive manufacturing. *Macromol Mater Eng* 302:1700143. <https://doi.org/10.1002/mame.201700143>
- Spoerk M, Arbeiter F, Raguž I, Weingrill G, Fischinger T, Traxler G, Schuschnigg S, Cardon L, Holzer C (2018) Polypropylene filled with glass spheres in extrusion-based additive manufacturing: effect of filler size and printing chamber temperature. *Macromol Mater Eng* 303:1800179. <https://doi.org/10.1002/mame.201800179>
- Maryan AS, Montazer M, Rashidi A, Rahimi MK (2013) Antibacterial properties of clay layers silicate: a special study of

- montmorillonite on cotton fiber. *Asian J Chem* 25:2889–2892. <https://doi.org/10.14233/ajchem.2013.14229>
14. Aumnate C, Limpanart S, Soatthiyanon N, Khunton S (2019) PP/organoclay nanocomposites for fused filament fabrication (FFF) 3D printing. *Express Polym Lett* 13:898–909. <https://doi.org/10.3144/expresspolymlett.2019.78>
 15. Qiu H, Si Z, Luo Y, Feng P, Wu X, Hou W, Zhu Y, Chan-Park MB, Xu L, Huang D (2020) The mechanisms and the applications of antibacterial polymers in surface modification on medical devices. *Front Bioeng Biotechnol* 8. <https://doi.org/10.3389/fbioe.2020.00910>
 16. Liu M, Bauman L, Nogueira CL, Aucoin MG, Anderson WA, Zhao B (2022) Antimicrobial polymeric composites for high-touch surfaces in healthcare applications. *Curr Opin Biomed Eng* 22:100395. <https://doi.org/10.1016/j.cobme.2022.100395>
 17. Turakhia B, Divakara MB, Santosh MS, Shah S (2020) Green synthesis of copper oxide nanoparticles: a promising approach in the development of antibacterial textiles. *J Coat Technol Res* 17:531–540. <https://doi.org/10.1007/s11998-019-00303-5>
 18. ASTM International (2014) ASTM D638–14, Standard test method for tensile properties of plastics. Annual Book of ASTM Standards
 19. ASTM I (2001) Standard practices for evaluating the resistance of plastics to chemical. Current 95
 20. ISO Standards (2008) Plastics-determination of water absorption; ISO 62:2008. 61010–1 © Iec:2001 2008
 21. Pawar RR, Lalmunsiam, Bajaj HC, Lee SM (2016) Activated bentonite as a low-cost adsorbent for the removal of Cu(II) and Pb(II) from aqueous solutions: batch and column studies. *J Indust Eng Chem* 34. <https://doi.org/10.1016/j.jiec.2015.11.014>
 22. Jin X, Zheng M, Sarkar B, Naidu R, Chen Z (2016) Characterization of bentonite modified with humic acid for the removal of Cu (II) and 2,4-dichlorophenol from aqueous solution. *Appl Clay Sci* 134:89–94. <https://doi.org/10.1016/j.clay.2016.09.036>
 23. Ding S Li, Sun Y Zhuang, Yang C Na, Xu B Hui (2009) Removal of copper from aqueous solutions by bentonites and the factors affecting it. *Min Sci Technol* 19. [https://doi.org/10.1016/S1674-5264\(09\)60091-0](https://doi.org/10.1016/S1674-5264(09)60091-0)
 24. Patel HA, Somani RS, Bajaj HC, Jasra RV (2006) Nanoclays for polymer nanocomposites, paints, inks, greases and cosmetics formulations, drug delivery vehicle and waste water treatment. *Bull Mater Sci* 29:133–145. <https://doi.org/10.1007/BF02704606>
 25. Mekewi MA, Darwish AS, Amin MS, Eshaq Gh, Bourazan HA (2016) Copper nanoparticles supported onto montmorillonite clays as efficient catalyst for methylene blue dye degradation. *Egypt J Pet* 25:269–279. <https://doi.org/10.1016/j.ejpe.2015.06.011>
 26. Gupta MK, Tandon PK, Pandey V, Afroz M, Malviya T (2023) Montmorillonite based copper oxide nanoparticles for the efficient remediation of phosphate and anti-bacterial activity against gram-negative bacteria. *Sep Sci Technol* 58:406–419. <https://doi.org/10.1080/01496395.2022.2121724>
 27. Chrissopoulou K, Anastasiadis SH (2011) Polyolefin/layered silicate nanocomposites with functional compatibilizers. *Eur Polym J* 47:600–613. <https://doi.org/10.1016/j.eurpolymj.2010.09.028>
 28. Bee S-L, Abdullah MAA, Bee S-T, Sin LT, Rahmat AR (2018) Polymer nanocomposites based on silylated-montmorillonite: a review. *Prog Polym Sci* 85:57–82. <https://doi.org/10.1016/j.progpolymsci.2018.07.003>
 29. Mahdavi E, Haghghi-Yazdi M, Mosavi Mashhadi M (2023) Coupled thermal stress and moisture absorption in modified a montmorillonite/copolymer nanocomposite: Experimental study. *Polym Test* 124:108092. <https://doi.org/10.1016/j.polymertesting.2023.108092>
 30. Rahman MdR, Hamdan S Bin, Hossen MdF (2018) The effect of clay dispersion on polypropylene nanocomposites: physico-mechanical, thermal, morphological, and optical properties. In: *Silica and Clay Dispersed Polymer Nanocomposites*. Elsevier, pp 201–257
 31. Sharma SK, Nayak SK (2009) Surface modified clay/polypropylene (PP) nanocomposites: effect on physico-mechanical, thermal and morphological properties. *Polym Degrad Stab* 94:132–138. <https://doi.org/10.1016/j.polymdegradstab.2008.09.004>
 32. Tan LJ, Zhu W, Zhou K (2020) Development of organically modified montmorillonite/polypropylene composite powders for selective laser sintering. *Powder Technol* 369:25–37. <https://doi.org/10.1016/j.powtec.2020.05.005>
 33. Northcutt LA, Orski SV, Migler KB, Kotula AP (2018) Effect of processing conditions on crystallization kinetics during materials extrusion additive manufacturing. *Polymer (Guildf)* 154:182–187. <https://doi.org/10.1016/j.polymer.2018.09.018>
 34. Gou J, Zhang L, Li C (2020) A new method combining modification of montmorillonite and crystal regulation to enhance the mechanical properties of polypropylene. *Polym Test* 82:106236. <https://doi.org/10.1016/j.polymertesting.2019.106236>
 35. Kumar V, Singh A (2013) Polypropylene clay nanocomposites. *Reviews in Chem Eng* 29. <https://doi.org/10.1515/revce-2013-0014>
 36. Cao J, Wen N, Zheng Y (2018) The preparation of calcium pime-late modified OMMT from natural Ca-montmorillonite and its application as β -nucleating agent for polypropylene. *Polym Test* 65:352–359. <https://doi.org/10.1016/j.polymertesting.2017.11.031>
 37. Chrissopoulou K, Altintzi I, Andrianaki I, Shemesh R, Retsof H, Giannelis EP, Anastasiadis SH (2008) Understanding and controlling the structure of polypropylene/layered silicate nanocomposites. *J Polym Sci B Polym Phys* 46:2683–2695. <https://doi.org/10.1002/polb.21594>
 38. Fischer C, Drummer D (2016) Crystallization and mechanical properties of polypropylene under processing-relevant cooling conditions with respect to isothermal holding time. *Int J Polym Sci* 2016:1–11. <https://doi.org/10.1155/2016/5450708>
 39. Carneiro OS, Silva AF, Gomes R (2015) Fused deposition modeling with polypropylene. *Mater Des* 83. <https://doi.org/10.1016/j.matdes.2015.06.053>
 40. Alexandre M, Dubois P (2000) Polymer-layered silicate nanocomposites: preparation, properties and uses of a new class of materials. *Mater Sci Eng R Rep* 28:1–63. [https://doi.org/10.1016/S0927-796X\(00\)00012-7](https://doi.org/10.1016/S0927-796X(00)00012-7)
 41. Kodgire P, Kalgaonkar R, Hambir S, Bulakh N, Jog JP (2001) PP/clay nanocomposites: effect of clay treatment on morphology and dynamic mechanical properties. *J Appl Polym Sci* 81:1786–1792. <https://doi.org/10.1002/app.1611>
 42. Morajane D, Sinha Ray S, Bandyopadhyay J, Ojijo V (2018) Impact of melt-processing strategy on structural and mechanical properties: clay-containing polypropylene nanocomposites. pp 127–154 https://doi.org/10.1007/978-3-319-97779-9_5
 43. Lavorgna M, Piscitelli F, Mangiacapra P, Buonocore GG (2010) Study of the combined effect of both clay and glycerol plasticizer on the properties of chitosan films. *Carbohydr Polym* 82:291–298. <https://doi.org/10.1016/j.carbpol.2010.04.054>
 44. Ladhari A, Ben Daly H, Belhadjsalah H, Cole KC, Denault J (2010) Investigation of water absorption in clay-reinforced polypropylene nanocomposites. *Polym Degrad Stab* 95:429–439. <https://doi.org/10.1016/j.polymdegradstab.2009.12.001>
 45. Moreira Martins PM, Gong T, de Souza AA, Wood TK (2020) Copper kills *Escherichia coli* persister cells. *Antibiotics* 9:506. <https://doi.org/10.3390/antibiotics9080506>

Publisher's Note Springer Nature remains neutral with regard to jurisdictional claims in published maps and institutional affiliations.

Springer Nature or its licensor (e.g. a society or other partner) holds exclusive rights to this article under a publishing agreement with the author(s) or other rightsholder(s); author self-archiving of the accepted manuscript version of this article is solely governed by the terms of such publishing agreement and applicable law.